TABLE IV: Comparison of Lattice and Continuous Forces in the Region 30 Å < R < 40 Å

	component		
	x	y	z
RMS(F_c)[a]	1.00×10^{-3}	3.66×10^{-3}	4.96×10^{-3}
RMS($F_l - F_c$)[a]	6.46×10^{-5}	1.56×10^{-4}	6.01×10^{-5}
RMS($F_l - F_c$)/RMS(F_c)	6.46×10^{-2}	4.26×10^{-2}	1.21×10^{-2}

[a] Forces in units of 0.6 kcal mol^{-1} Å^{-1}.

TABLE V: Dependence of Reactive Collision Frequency on Time Step[a]

	collision frequency	
time step	lattice method	continuous method
$4\Delta t$	0.166 ± 0.018	0.154 ± 0.016
$2\Delta t$	0.184 ± 0.017	0.164 ± 0.015
Δt	0.178 ± 0.018	0.196 ± 0.018
$\Delta t/2$	0.196 ± 0.016	0.208 ± 0.018
$\Delta t/4$	0.180 ± 0.016	0.170 ± 0.015

[a] Based on 500 trajectories for each time step. The 76-charge model of SOD with b = 40 Å and q = 50 Å is used in each case.

are very close to the continuously computed forces for R > 40 Å.

In the region 30 Å < R < 40 Å, we have compared the lattice forces and continuous forces at random points on actual trajectories starting at 40 Å. The results for about 1000 points are given in Table IV. As can be seen from this table, the ratio of RMS deviation to RMS force has a maximum value of 0.06. This indicates that the relevant lattice forces are very close to the continuous forces even in this potentially troublesome region.

Comparison of successively calculated forces in typical trajectories shows that the change in force is small in each time step Δt. This can also be established by comparing reactive collision frequencies computed by using different Δt values. The results of such calculations are given in Table V. It can be seen from this table that reducing Δt by a factor of 2 or more does not change the collision frequency appreciably. Even increasing Δt by a factor of 2 or 4 does not change the collision frequency significantly, indicating that the Δt values used in these simulation are small enough that the dynamics of the trajectories faithfully reflect the intermolecular forces.

4. Concluding Remarks

This paper has introduced and demonstrated the utility of a Brownian dynamics trajectory approach for calculating diffusion-controlled rate constants for reactant molecules that have numerous interactions. The novel feature of this approach consists of the use of net forces stored for an array of lattice points to avoid the need to recompute the whole set of intermolecular interactions at each step of each trajectory. Clearly, the approach introduced here could be extended in a variety of ways, e.g., by storing information on hydrodynamic interactions as well as on the forces. The lattice approach is also naturally suited for studying diffusional motion in electrostatic fields that are themselves evaluated by numerical methods (e.g., when simulations are used to determine mean fields in the presence of mobile co- and counterions). A limitation of this approach is that it may be difficult to include effects due to *internal* mobility of the reactants, although averaging over internal motions may be possible for sufficiently large reactant separations.

Although the SOD–O_2^- system was introduced here only for illustrative purposes, it is also of interest that the results obtained for detailed charge distributions on the enzyme confirm the validity of previous results based on simplified models for the enzyme. For other systems, it may happen that simplified models will be inadequate and the approach described in this paper will be required to obtain accurate rate constants. In addition to the situations mentioned above, this is likely to be the case for reactants that are less symmetrical than SOD, which as a nearly spherical dimer with identical subunits has a field that is well approximated over the relevant diffusion space by low-order multipoles.

Acknowledgment. This work was supported by the Robert A. Welch Foundation and the NIH. J.A.M. is a Sloan Fellow and the recipient of Dreyfus Teacher–Scholar and NIH RCDA Awards. S.A.A. is the recipient of an NSF Presidential Young Investigator Award and a Dreyfus Grant for Newly Appointed Faculty in Chemistry.

Registry No. Superoxide dismutase, 9054-89-1; superoxide, 11062-77-4.

Vibrational Energy Distributions of Singlet Methylene from Photolyses of Ketene, Ketene-d_2, Diazomethane, and Diazomethane-d_2 at Several Wavelengths. A Chemically Activated Methylcyclobutane Study

W. C. Mahone, W. Kolln, and J. W. Simons*

Chemistry Department, New Mexico State University, Las Cruces, New Mexico 88003
(Received: January 30, 1985)

The energy distributions of singlet methylene upon reaction with cyclobutane have been determined for methylene from photolysis of ketene and ketene-d_2 at 214 nm, diazomethane at 436, 366, 337, and 229 nm, and diazomethane-d_2 at 366 nm. Earlier results for diazomethane photolyses at 436 and 366 nm are extended and reanalyzed in terms of a more recent stepsize determination for collisional deactivation of chemically activated methylcyclobutane. The widths of the singlet methylene energy distributions were found to increase with increasing photon energy and with deuterium substitution. An extensive analysis in terms of a statistical energy partitioning model for photodissociation of ketene and diazomethane is given and discussed.

Introduction

Several years ago,[1] it was shown that an apparent discrepancy between diazomethane-generated $CH_2(^1A_1)$ chemical activation data, leading to a very large collisional deactivation stepsize (~30 kcal mol^{-1}),[2] and ketene-generated data, giving a much smaller stepsize (~10 kcal mol^{-1})[2] for polyatomic deactivators, was due to the assumption of monoenergetic activated molecules. This

(1) T. H. Richardson and J. W. Simons, *Chem. Phys. Lett.*, **41**, 168 (1976).

(2) J. W. Simons, B. S. Rabinovitch, and D. W. Setser, *J. Chem. Phys.*, **41**, 800 (1964); D. W. Setser, B. S. Rabinovitch, and J. W. Simons, *ibid.*, **40**, 1751 (1964).

0022-3654/85/2089-3902$01.50/0

discrepancy was resolved by including a broad distribution of energies, which then allowed a smaller stepsize, for the higher energy diazomethane systems. Since that time a number of chemical activation studies of $CH_2(^1A_1)$ energy distributions from ketene and diazomethane photolyses have appeared.[3-6] What has emerged are some general trends such as distributions that vary with photon energy and $CH_2(^1A_1)$ precursor in a qualitatively expected way. The quantitative aspects of these distributions are not well established. The detailed shapes of the distributions and their relationship to the photodissociation energy partitioning in the precursors are important unanswered questions.

In this study our earlier chemically activated methylcyclobutane work from reaction of $CH_2(^1A_1)$ with cyclobutane is extended to include ketene photolyses at 214 nm and diazomethane photolyses at 229 nm in order to examine the $CH_2(^1A_1)$ energy distributions from ketene and diazomethane photolyses in their short-wavelength absorption bands. The effect of deuterium substitution is also examined in a study utilizing CD_2CO photolyses at 214 nm and CD_2N_2 photolyses at 366 nm.

Previous work on diazomethane photolyses at 436 and 366 nm is extended, and new results at 337 nm are presented and reanalyzed in light of more recent work on the very important collisional deactivation stepsize determination in this chemically activated methylcyclobutane system.

Experimental Method

Materials. Cyclobutane, ketene, and oxygen were prepared as previously described.[7] Diazomethane was prepared by treating *N*-methyl-*N*-nitroso-*p*-toluenesulfonamide with a strong base (NaOH) by using 1,4-butanediol as a solvent. Diazomethane-d_2 was prepared by a similar treatment of the deuterated sulfonamide with a deuterated base (NaOD). The 1,4-butanediol was allowed to mix with excess D_2O for 72 h in order to exchange all exchangeable H atoms. The excess water was then removed by evaporation. Mass spectroscopic analysis of the ethylene formed from diazomethane-d_2 photolysis gave an isotopic composition of 7% H which leads to 13% $CDHN_2$ and 87% CD_2N_2. The diazomethane and diazomethane-d_2 were stored in solution with dibutyl phthalate at 77 K for later use.

Procedure. Mixtures of ketene (diazomethane), cyclobutane, and oxygen in the approximate ratios of 1:10:2 were prepared in a high-vacuum system. These mixtures were loaded into reactors constructed from Pyrex Erlenmeyer flasks with Pyrex windows for the diazomethane 436-, 366-, and 337-nm photolyses systems. Quartz reactors were used for the 229-nm diazomethane and 214-nm ketene photolyses. All stopcocks in the vacuum system were of the greaseless, Teflon plug (O-ring) type. Total pressures were varied by varying reactor volumes and amounts of reactants. The source of the 436- and 366-nm radiation was a 500-W Osram point source mercury lamp in an Oriel Optics housing with a quartz lens system. Wavelength isolation was achieved by the use of colored glass prefilters in series with a Bausch and Lomb $^1/_4$-m high-intensity monochromator. An Esco Products filter no. 5970 was used as the prefilter in the 366-nm experiments. The 436-nm prefilter was a combination of filter no. 3389 (yellow) and Schott glass no. BG12 (blue).

The 337-nm radiation source was the unfocused output of a Molectron UV-12 nitrogen laser. The 214-nm radiation was obtained from a Phillips 25-W zinc lamp, and the 229-nm radiation was obtained from a Phillips 25-W cadmium lamp. Both the zinc and cadmium radiation were coupled to a $^1/_4$-m Jarrel Ash monochromator (Model 82-410) with 2-mm slits. Photolysis times varied from 2 to 48 h depending on the pressure, reaction vessel size, and radiation source.

TABLE I: k_4 (10^9 s^{-1}) at S/D = 2 for Various Systems and k_H/k_D Ratios

system	k_4 (S/D = 2)[a]	
CH_2N_2, 436 nm	2.3 ± 0.1	
CH_2N_2, 366 nm	3.4 ± 0.2	
CH_2N_2, 337 nm	4.5 ± 0.2	
CH_2N_2, 229 nm	10.5 ± 0.1	
CH_2CO,[b] 214 nm	5.3 ± 0.3	
CD_2CO,[b] 214 nm	5.9 ± 0.3	
CD_2N_2, 366 nm	3.1 ± 0.04	
	k_H/k_D	
	S/D = 1-2	S/D = 0.03
ketene, 214 nm	0.91	1.03
diazomethane, 366 nm	1.12	1.14

[a] Units of 10^9 s^{-1}. [b] Values at S/D = 1.

The analysis of the reaction products as well as a description of the analytical apparatus can be found in our earlier paper.[7] The gas chromatographic analyses were calibrated with mixtures of known composition. Dark reactions were found to yield no propylene or methylcyclobutane, the products of interest in this work.

Corrections to Data. The ketene and ketene-d_2 preparation and purification procedure[7] did not eliminate a small propylene impurity; consequently, a correction to the propylene analyses in the 214-nm ketene and ketene-d_2 data was necessary. The correction for each experiment was determined from a propylene impurity vs. ketene sample size curve. The relative magnitude of the correction varied from less than 10% of the total amount of propylene at low pressures to not over 50% at the highest pressures.

A correction for the 13% $CHDN_2$ in the CD_2N_2 was derived based on the assumption that CHD results would be halfway between CD_2 and CH_2 results. At a given pressure the desired CD_2 results would be given by (the 87% CD_2 + 13% CHD result) divided by 0.935 minus 0.07 times the corresponding CH_2 result. In practice this correction was quite small and not an important source of error.

Experimental Results

A mechanism that provides an adequate description of the dynamic processes that occur in the photolysis of diazomethane or ketene in excess cyclobutane is as follows

$$CH_2CO \text{ or } CH_2N_2 \xrightarrow{h\nu} CH_2(^1A_1) + CO \text{ or } N_2 \quad (1)$$

$$CH_2(^1A_1) + CB \xrightarrow{k_2} MCB^* \quad (2)$$

$$MCB^* \xrightarrow{w} \xrightarrow{w} \xrightarrow{w} \xrightarrow{w} MCB \quad [S] \quad (3)$$

$$MCB^* \rightarrow \rightarrow \rightarrow \rightarrow CH_3CHCH_2 + C_2H_4 \quad [D] \quad (4)$$

where CB is cyclobutane, MCB is methylcyclobutane, MCB* is methylcyclobutane with internal energy in excess of that needed for decomposition, w is the gas kinetic collision frequency of MCB* with the bath gases,[7] and k_4 is defined by the following equation:

$$k_4 = w(D/S) \quad (I)$$

If process 3 were a single-step process and MCB* were a monoenergetic species, then k_4 would truly be a constant. However, since neither of the above is true, variations of k_4 with pressure was observed. These variations can be used to derive information about process 3 as well as the MCB* initial energy distribution.

The decomposition to stabilization ratio, D/S, for the 214-nm ketene and the diazomethane systems was determined directly by measuring the relative amounts of propylene and MCB produced by processes 3 and 4. In our earlier work[7] on $CH_2(^1A_1)$ from *low-energy ketene photolyses* it was necessary to utilize an internal standard to monitor the total $CH_2(^1A_1)$ reaction since the propylene amounts were found not to be a valid measure of decomposition. In the present work, utilizing *diazomethane and higher*

(3) T. H. Richardson and J. W. Simons, *J. Am. Chem. Soc.*, **100**, 1062 (1978).
(4) R. J. Wolf and W. L. Hase, *J. Phys. Chem.*, **82**, 1850 (1978).
(5) W. S. Kolln, M. Johnson, D. E. Peebles, and J. W. Simons, *Chem. Phys. Lett.*, **65**, 85 (1979).
(6) I. Szilágyi, L. Zatotai, T. Bercés, and F. Márta, *J. Phys. Chem.*, **87**, 3694 (1983).
(7) J. W. Simons and W. C. Mahone, *J. Phys. Chem.*, submitted for publication.
(8) Deleted in proof.

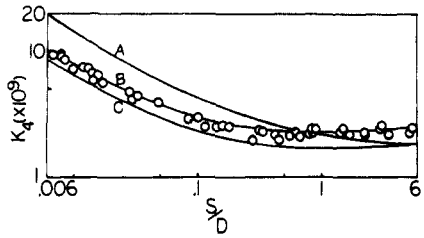

Figure 1. k_4 (s^{-1}) vs. S/D for the 436-nm CH_2N_2 system: curve A, 1.22 × calculated curve for m = 6 kcal mol^{-1} and g_2 = 1; curve B, 1.22 × calculated curve from best fit distribution; curve C, 1.22 × calculated curve from the statistical distribution.

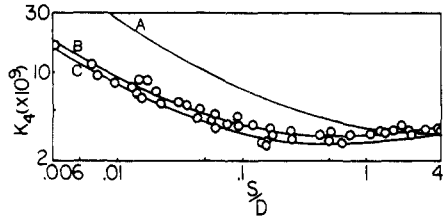

Figure 2. k_4 (s^{-1}) vs. S/D for the 366-nm CH_2N_2 system: curve A, 1.22 × calculated curve for m = 6 kcal mol^{-1} and g_3 = 1; curve B, 1.22 × calculated curve from best fit distribution; curve C, 1.22 × calculated curve from the statistical distribution.

energy ketene photolyses, some internal standard experiments were performed and were found to agree with propylene/MCB measurements so an internal standard was not necessary here.

Averaged values of k_4 at S/D = 2 are given in Table I for all systems studied here. These are averages of data between S/D = 1 and 3, except for the 214-nm ketene system where the average was around S/D = 1 because of the difficulty in obtaining high S/D data. This difficulty was primarily due to the propylene impurity becoming a major fraction of the propylene from process 3 at high temperatures.

The variation of k_4 with S/D for the 436-nm CH_2N_2 system is shown in Figure 1. This is an expanded data set over that presented earlier for this system but is in good agreement with the earlier work.[3] On inspection we see that k_4 remains relatively constant from high S/D down to an S/D of about 0.4. As S/D is further reduced, an increase in k_4 is observed. We note that this increase begins at a smaller S/D and is less steep than for the lower energy systems.[7] Previous investigations[3] have shown that this behavior is due to the width of the initial energy distribution for the energized molecules, MCB*.

The 366-nm CH_2N_2 data shown in Figure 2 reveal a slight decline in k_4 as S/D is decreased, reaching a minimum around S/D = 0.3, followed by an increase in k_4 which is less than that observed for the 436-nm data. These effects can be explained by a broader distribution of energies for MCB* in the 366-nm system than for the 436-nm system.[3] These 366-nm results represent a greatly expanded data set that is in good agreement with our earlier results for the same system.[7]

Comparison of the 436- and 366-nm diazomethane results in this work to those recently presented for chemically activated 1,2-dimethylcyclopropane[6] reveals a major discrepancy. The decrease in the rate in going from high to intermediate S/D values for the dimethylcyclopropane work is many times larger than that observed in this work. Since the dimethylcyclopropane work requires the use of an internal standard to determine S/D, which may be unreliable at large S/D values[7] where one is determining the small difference of two large experimental quantities, we feel that the behavior observed here, where S and D are directly measured, is more likely to be correct.

The 337-nm data presented in Figure 3 decline somewhat more with S/D than the 366-nm data, giving a minimum around S/D = 0.2 and then increasing with further decrease in S/D. This suggests a higher average energy and a broader initial energy distribution for the 337-nm system.

The 229-nm data in Figure 4 exhibit a large decline in k_4 with decreasing S/D, reaching a minimum of $0.5k_4$(S/D=2) at S/D = 0.1 and then slowly increasing to approximately $1.5k_4$(S/D=2) at S/D ~ 0.006. Following earlier interpretations, these results indicate a very broad distribution of energies for MCB* in this system.[3]

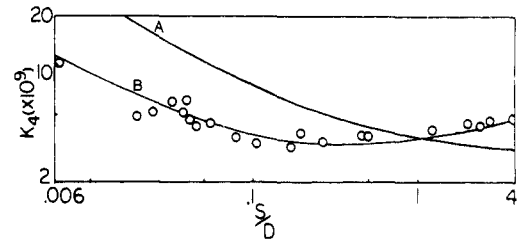

Figure 3. k_4 (s^{-1}) vs. S/D for the 337-nm CH_2N_2 system: curve A, 1.22 × calculated curve for m = 6 kcal mol^{-1} and g_3 = 1; curve B, 1.22 × calculated curve from best fit distribution; curve C, calculated curve from statistical distribution is identical with curve B.

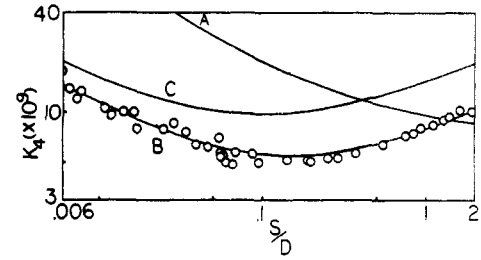

Figure 4. k_4 (s^{-1}) vs. S/D for the 229-nm CH_2N_2 system: curve A, 1.22 × calculated curve for m = 6 kcal mol^{-1} and g_5 = 1; curve B, 1.22 × calculated curve from the best fit distribution; curve C, 1.22 × calculated curve from the statistical distribution.

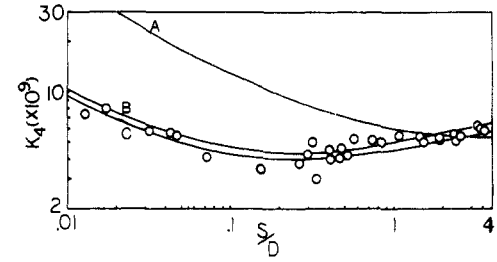

Figure 5. k_4 (s^{-1}) vs. S/D for the 214-nm CH_2CO system: curve A, 1.22 × calculated curve for m = 6 kcal mol^{-1} and g_4 = 1; curve B, 1.22 × calculated curve from best fit distribution; curve C, 1.22 × calculated curve from the statistical distribution.

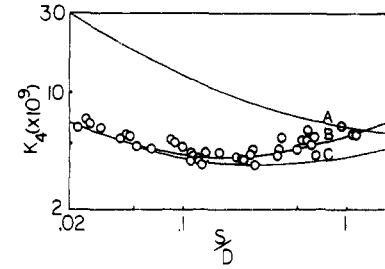

Figure 6. k_4 (s^{-1}) vs. S/D for the 214-nm CD_2CO system: curve A, 1.22 × calculated curve for m = 6 kcal mol^{-1} and g_6 = 1; curve B, 1.22 × calculated curve from best fit distribution; curve C, 1.22 × calculated curve from statistical distribution.

A similar observation can be made from the 214-nm CH_2CO data in Figure 5. Inspection of the curvature places it somewhere between the 337- and the 229-nm diazomethane system.

The CD_2CO 214-nm data are presented in Figure 6. Due to reduced product yield we were unable to cover a large S/D range with this system. This reduction in product yield upon isotopic substitution was observed in all of the deuterated systems. Since we assume that the CH_2 and CD_2 reaction cross sections with cyclobutane are very nearly the same, this effect is probably the result of a reduced photolysis efficiency in the methylene precursors upon isotopic substitution, leading to a reduction in the rate of

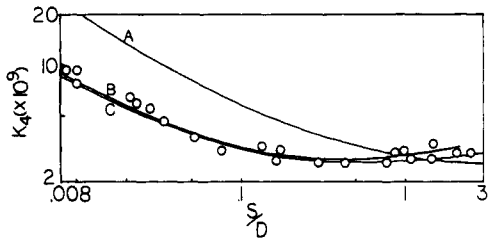

Figure 7. k_4 (s^{-1}) vs. S/D for the 366-nm CD_2N_2 system: curve A, 1.22 × calculated curve for m = 6 kcal mol^{-1} and g_4 = 1; curve B, 1.22 × calculated curve from best fit distribution; curve C, 1.22 × calculated curve from statistical distribution.

$CD_2(^1A_1)$ production. A comparison with the CH_2CO 214-nm system indicates a slightly higher k_4 at S/D = 1 (k_H/k_D = 0.91) and a slightly lower k_4 at lower S/D (k_H/k_D = 1.03 at S/D = 0.03). This represents a similar although somewhat smaller variation in isotope effect than that observed earlier from the low-energy 313-nm ketne system.[7]

The 366-nm CD_2N_2 data shown in Figure 7 give a small normal isotope effect (k_H/k_D = 1.13) over the entire S/D range. A comparison of the isotope effects for 366-nm diazomethane and for 214-nm ketene photolyses may reveal fundamentally different isotopic behavior, although all of these results fall within 10–15% of k_H/k_D = 1.0.

Calculational Results

A model suitable for interpretation of these results has been presented earlier.[3,7] This model contains five important quantities: w, the collision frequency; m, the collisional energy removal stepsize; k_i, the specific rates for dissociation from each excited level; f_i, the thermal energy distribution for the excited molecules; and g_v, the population numbers of the vibrational levels of the reacting singlet methylenes. The collisional energy removal stepsize actually represents the mean value of a Gaussian distribution of stepsizes which is assumed to be constant at all of the energies of this study. Thus, the value of m = 6 ± 2 kcal mol^{-1} determined for the 337-nm ketene photolysis system[7] is assumed to apply for all systems in this work.[3,7] The populations, g_v, of the various methylene vibrational levels were varied so as to fit calculated k_4 vs. S/D curves to the data for the various systems. It is noted that all calculated k_4 vs. S/D curves in this work are multiplied by a factor of 1.22 which was required to bring the g_v = 1, m = 6 kcal mol^{-1} calculation into absolute agreement with the 337-nm CH_2CO data as discussed previously.[7]

The $CH_2(^1A_1)$ vibrational model used gives a set of levels with a constant 4 kcal mol^{-1} spacing,[3,7] and the $CD_2(^1A_1)$ model similarily gives a 3 kcal mol^{-1} vibrational level spacing.[7] As in our previous work,[3] the sets of g_v were generated with a Gaussian function for which the position of the maximum and the width of the function were varied. The resultant g_v distributions were skewed since the Gaussians were necessarily truncated at v = 0. It is emphasized that any g_v generating function with a variable maximum position and width would suffice and the Gaussian function was merely convenient to use.

The fact that levels in which the methylene vibrational energy, $E_v = 4v$, exceeds E_{xs} (see Table II) must have zero population is not a serious restriction for these high-energy systems, as will be seen later.

436-nm CH_2N_2 Photolysis System. The "best fit" calculated curve through the 436-nm data is shown in Figure 1. The set of g_v giving this curve is represented in Figure 8. Also shown in Figure 1 is a calculated curve for monoenergetic $CH_2(^1A_1)$, g_2 = 1, with approximately the same $\langle E_v \rangle$ as the best fit curve. Comparison of the two curves clearly demonstrates the importance of a distribution of methylene vibrational energies in fitting the data for this system. It is noted that the g_v values for the best fit distribution in Figure 8 are quite small in the vicinity of $v_{max} = E_{xs}/4$, and hence the requirement that g_v = 0 for $v > E_{xs}/4$ is easily met and the rather large uncertainty in E_{xs} (Table II) introduces no uncertainty in the set of g_v values.

TABLE II: Energetics[a]

system	E_{xs}[b]	$\langle E_v \rangle$[c]	$\langle E_v \rangle / E_{xs}$[d]	ref
CH_2CO, 337 nm	0.8 ± 2	0		7
CD_2CO, 337 nm	0.9 ± 2	0.9		7
CH_2CO, 334 nm	1.6 ± 2	0		7
CD_2CO, 334 nm	1.7 ± 2	0.9		7
CH_2CO, 313 nm	7.3 ± 2	1.2	0.13–0.23 (0.16)	7
CD_2CO, 313 nm	7.4 ± 2	3.2	0.32–0.59 (0.43)	7
CH_2CO, 214 nm	49.5 ± 2	14.9	0.30 ± 0.01	this work
CD_2CO, 214 nm	49.6 ± 2	18.1	0.37 ± 0.01	this work
CH_2N_2, 436 nm	25 ± 10	8.5	0.25–0.57 (0.34)	this work
CH_2N_2, 366 nm	37.6 ± 10	11.1	0.23–0.40 (0.30)	this work
CD_2N_2, 366 nm	37.7 ± 10	12.6	0.26–0.46 (0.33)	this work
CH_2N_2, 337 nm	44.3 ± 10	12.3	0.23–0.36 (0.28)	this work
CH_2N_2, 229 nm	84.3 ± 10	19.0	0.20–0.26 (0.23)	this work

[a] All energies are in kcal mol^{-1}. [b] $E_{xs} = h\nu - \Delta H_0°$ (1) + E_{th}, where E_{th} = 0.5 kcal mol^{-1} for CH_2X and E_{th} = 0.6 kcal mol^{-1} for CD_2X (X = CO or N_2); $\Delta H_0°$ (1) = $\Delta H_f°_0[CH_2(^1A_1)]$ + $\Delta H_f°_0$ [X] − $\Delta H_f°_0$-$[CH_2X]$, $\Delta H_f°_0[CH_2N_2]$ = 60 ± 10 kcal mol^{-1} (ref 9); other heats are discussed in ref 7. [c] The average vibrational energy of CH_2 or CD_2. $\langle E_v \rangle = 4\sum v g_v$ for CH_2, $\langle E_v \rangle = 3\sum v g_v$ for CD_2. [d] Values in parentheses are for the preferred values of E_{xs}.

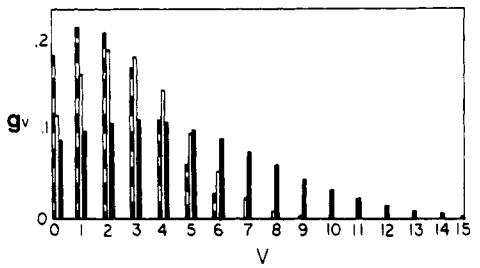

Figure 8. Normalized population vibrational levels of $CH_2(^1A_1)$ for CH_2N_2 systems. ▭▪▭ refers to the best fit distribution for the 436-nm CH_2N_2; ▭ refers to the best fit distribution for the 366-nm CH_2N_2; and ▬ refers to the best fit distribution for the 229-nm CH_2N_2.

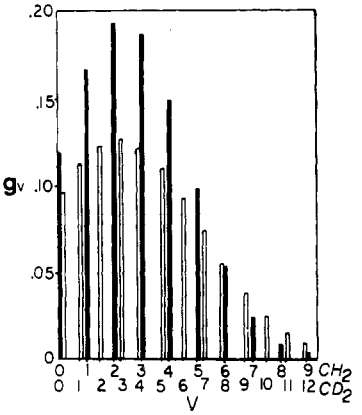

Figure 9. Normalized vibrational level populations for methylene from 366-nm CH_2N_2 and CD_2N_2 photolyses. ▬ refers to CH_2N_2 and ▭ refers to the CD_2N_2. The relative positions of the CH_2 and CD_2 vibrational levels are on the same energy scale.

The set of g_v and the value of $\langle E_v \rangle$ found in this work with an expanded data set, m = 6 kcal mol^{-1} and $\Delta H_f°_0[CH_2(^1A_1)]$ = 101 kcal mol^{-1}, are very similar to our earlier results[3] with m = 4 kcal mol^{-1} and $\Delta H_f°_0[CH_2(^1A_1)]$ = 99 kcal mol^{-1}.

366-nm CH_2N_2 Photolysis System. The best fit calculated curve through the 366-nm data is shown in Figure 2. The set of g_v giving this curve is also represented in Figure 8. A calculated curve for a monoenergetic methylene system, g_3 = 1, with E_v near the $\langle E_v \rangle$ (see Table II) of the best fit 366-nm curve is also shown in Figure 2. Comparison of these curves demonstrates the need for an even broader distribution of energies than at 436 nm. We also note that this broader distribution duplicates the minimum in the k_4 vs. S/D data observed for the 366-nm system.

As in the case of the 436-nm CH_2N_2 system the set of g_v and the value of $\langle E_v \rangle$ for the 366-nm system in this work are in close

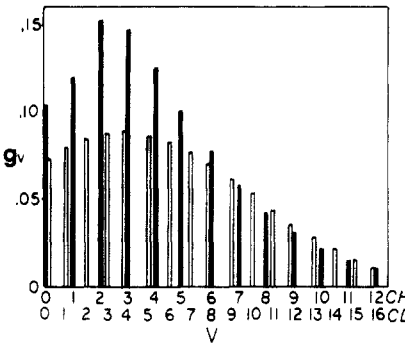

Figure 10. Normalized vibrational level populations for methylene from 214-nm CH_2CO and CD_2CO photolyses. ▬ refers to CH_2CO and ▭ refers to CD_2CO. The relative positions of the CH_2 and CD_2 vibrational levels are on the same energy scale.

agreement with our earlier work.[3]

337-nm CH_2N_2 Photolysis System. The best fit calculated curve through the 337-nm CH_2N_2 data is shown in Figure 3. The set of g_v (not shown) giving this curve is slightly broader than the 366-nm distribution, resulting in the slightly larger $\langle E_v \rangle$ in Table II.

229-nm CH_2N_2 Photolysis System. The best fit calculated curve through the 229-nm data is shown in Figure 4. Figure 8 shows that the set of g_v giving the best fit curve in Figure 4 is significantly broadened relative to the 436- and 366-nm systems. When the "best fit" curve is compared to the calculated curve for monoenergetic $CH_2(^1A_1)$, $g_5 = 1$, in Figure 4, the large effect of the broad distribution for this system is clearly demonstrated. It is noted that the significant minimum in the k_4 vs. S/D data is quantitatively explained.

214-nm CH_2CO Photolysis System. The best fit curve for the 214-nm ketene system is shown in Figure 5. This system, which has an E_{xs} (see Table II) between that of the 366- and the 229-nm diazomethane systems, gives a distribution which has an average energy between these two systems. The g_v responsible for this distribution is shown in Figure 10.

214-nm CD_2CO Photolysis System. The best fit curve through the 214-nm CD_2CO data is shown in Figure 6. The set of g_v which gave rise to this curve is shown in Figure 10 also. The distribution for the heavy system is broader than for the light system. From Table II we can see that the $\langle E_v \rangle$ is higher for the isotopic system.

366-nm CD_2N_2 Photolysis System. The best fit curve through the 366-nm CD_2N_2 system is shown in Figure 7. The g_v which gave rise to this curve is shown in Figure 9 along with the g_v for the 366-nm CH_2N_2 system. The average energy for the deuterated system is slightly higher than for the light system.

Discussion

It is noted from Figures 8–10 that the width of the $CH_2(^1A_1)$ energy distributions and from Table II that the average vibrational energy, $\langle E_v \rangle$, of the reacting methylenes increase with increasing photon energy. This general result is in agreement with earlier work.[1-7] This observed qualitative behavior is consistent with a statistical redistribution of excess energy among the internal modes of the methylene precursor prior to dissociation. The fact that all of the distributions in this work are relatively wide is in itself also in agreement with a statistical redistribution of energy.

It is also noted that $\langle E_v \rangle$ for $CH_2(^1A_1)$ from the 436- and 366-nm CH_2N_2 photolyses in Table II are 40% less than those determined in a recent study of chemically activated dimethylcyclopropane.[6] As discussed in the Experimental Results section, we believe this discrepancy is probably due to the strong dependence of the dimethylcyclopropane results on very high S/D data, which are very uncertain. This unlikely large $\langle E_v \rangle$, due to unlikely large widths of the energy distributions, then requires a rather small value of m ($\sim$3 kcal mol^{-1}) to fit the low S/D data.[6]

Energy Partitioning. All of the systems in this work taken together suggest that the reacting $CH_2(^1A_1)$ carries about 30% (see Table II) of the excess energy into the reaction with cyclobutane. There is a large uncertainty in the fraction of the excess energy that ends up in the $CH_2(^1A_1)$ from diazomethane at the time of reaction due to a large uncertainty ($\pm$10 kcal mol^{-1}) in the heat of formation of diazomethane. However, the most recent discussion of this quantity suggests that the heat of formation of diazomethane is approximately 60 kcal mol^{-1}.[9] Using this value, one notes from Table II that the fraction of the excess energy that is contained in the $CH_2(^1A_1)$ at the time of reaction tends to decrease with increasing E_{xs} for the diazomethane systems. This behavior could reflect changes in the energy redistribution process which occurs in the diazomethane prior to dissociation, or it may simply be that the higher the energy of the methylenes the larger the fraction of collisional energy loss prior to reaction with cyclobutane. For the 214-nm CH_2CO photolysis system, for which E_{xs} is accurately known, an average of 30% of the excess energy appears as vibrational energy in the methylene, i.e. about the same as for the 436-, 366-, and 337-nm diazomethane systems by using the preferred $\Delta H_f[CH_2N_2]$ value.

Recent studies of 193-nm ArF laser photolyses of CH_2CO have yielded CO vibrational[10] and rotational[11] distributions and average energies. These average energies give the fractions of the excess energy going into the CO vibration, $f_v^{CO} = 0.10$, and into the CO rotations, $f_r^{CO} \geq 0.22$, combined with the above result, $f_v^{CH_2} \geq 0.30$, leave $\leq$38% of the excess energy to be partitioned among the $CH_2(^1A_1)$ rotations and relative translation of the CH_2 and CO fragments. The fact that the excess energy is spread throughout the various modes of the dissociating fragments is indicative of a redistribution of energy prior to dissociation.

Isotope Effects. It is seen from Table II and Figures 9 and 10 that deuterium substitution on ketene (214-nm CD_2CO photolyses) and on diazomethane (366-nm CD_2N_2 photolyses) results in wider vibrational energy distributions and higher average energies for $CD_2(^1A_1)$ at the time of reaction than for the corresponding undeuterated systems. This is due to an increased number of $CD_2(^1A_1)$ vibrational states relative to $CH_2(^1A_1)$ in the same excess energy range. This is an energy partitioning isotope effect which acts to increase k_4 in the deuterated systems. In addition, there is a normal secondary kinetic isotope effect on k_4 due to deuterium substitution in the chemically activated methycyclobutane; i.e., this effect would act to lower k_4.[12] These two compensating isotope effects result in the minimal change in k_4 shown in Table I for CD_2 vs. CH_2 results in these high-energy systems.

Statistical Partitioning Model. Statistical energy partitioning calculations were done for all the systems in this study. The calculations utilize an RRKM theory based model originally proposed by Lin and Rabinovitch[13] and given explicitly for CH_2CO and CH_2N_2 photodissociation in our earlier work.[7] An assumption in our model is that photodissociation occurs via a vibrationally excited ground electronic state since ground-state vibrational frequencies for both CH_2CO[14] and CH_2N_2[15] are used in the calculations. In fact, activated complex frequencies should be used, but in the absence of a knowledge of these we use molecular frequencies.

The k_4 vs. S/D curve for the 214-nm CH_2CO photolysis system calculated from the statistical model distribution of $CH_2(^1A_1)$ vibrational energies is given in Figure 5. This curve is slightly below the data since the statistical model distribution is narrower than the "best fit" distribution. The statistical $\langle E_v \rangle$ = 13.1 kcal mol^{-1} is also slightly smaller than for the best fit distribution (Table II). Fujimoto et al. did an identical statistical calculation for the CO vibrational energy distribution from CH_2CO photolysis at 193

(9) A. H. Laufer and H. O'Kabe, *J. Am. Chem. Soc.*, **93**, 4137 (1971).
(10) G. T. Fujimoto, M. E. Umstead, and M. C. Lin, *Chem. Phys.*, **65**, 197 (1982).
(11) R. N. Rosenfeld and B. I. Sonobe, *J. Am. Chem. Soc.*, **105**, 1661 (1983).
(12) P. J. Robinson and K. A. Holbrook, "Unimolecular Reactions", Wiley-Interscience, New York, 1972; p 291.
(13) Y. N. Lin and B. S. Rabinovitch, *J. Phys. Chem.*, **74**, 1769 (1970).
(14) A. P. Cox and A. S. Eshitt, *J. Chem. Phys.*, **38**, 1636 (1963).
(15) B. L. Crawford Jr., Wilt Fletcher, and D. A. Ramsay *J. Chem. Phys.*, **19**, 406 (1951).

nm and found good agreement with their data.[10] In general, the statistical calculation seems to adequately fit both the $CH_2(^1A_1)$ vibrational energy distribution from CH_2CO photolysis at 214 nm and the CO vibrational energy distribution from CH_2CO photolysis at 193 nm. A note of caution is necessary due to the possibility of partial collisional relaxation of our experimental $CH_2(^1A_1)$ distributions.

For the ketene systems there is both experimental and theoretical evidence for photodissocation via a vibrationally excited ground electronic state,[10,11,16] and hence there is reason to expect this basic assumption of our statistical calculation to be valid. For diazomethane there is no experimental evidence for photodissociation via a vibrationally excited ground state so our statistical calculations for the diazomethane system may be based on an invalid assumption. There are, however, theoretical arguments for CH_2N_2 dissociation into $CH_2(^1A_1) + N_2$ occurring via a vibrationally excited ground state.[17] The diazomethane statistical calculations are also quantitatively uncertain due to the uncertainty in the heat of formation of diazomethane.

The k_4 vs. S/D curve, for the 436-nm photolysis of CH_2N_2, calculated from the statistical distribution is seen in Figure 1 to be significantly below the data (~30%). This statistical distribution gives $\langle E_v \rangle$ = 6.2 kcal mol^{-1} compared to 8.5 kcal mol^{-1} for the best fit distribution.

The k_4 vs. S/D curve for the 366-nm photolysis of CH_2N_2 calculated from the statistical distribution is seen in Figure 2 to be below but somewhat closer to the data than the 436-nm system. The statistical distribution gives $\langle E_v \rangle$ = 10.2 kcal mol^{-1} which is only slightly less than the value for the best fit distribution (Table II).

The k_4 vs. S/D curve for the 337-nm photolysis of CH_2N_2 calculated from the statistical distribution is very close to the best fit distribution curve (Figure 3) and gives a similar value of $\langle E_v \rangle$ = 12.1 kcal mol^{-1}.

The k_4 vs. S/D curve for the 229-nm photolysis of CH_2N_2 calculated from the statistical model distribution is considerably above the data and the best fit distribution as shown in Figure 4. The statistical model distribution gives $\langle E_v \rangle$ = 24.8 kcal mol^{-1} which is also much larger than the value in Table II for the best fit distribution.

Given the uncertainty in the heat of formation of CH_2N_2, the fit of the statistical model distributions to the 436-, 366-, and 337-nm CH_2N_2 photolysis data is adequate. However, this is not the case for the 229-nm CH_2N_2 photolyses. This may be due to the fact that since 229-nm photons produce a different excited state of CH_2N_2 than do 436-, 366-, or 337-nm photons, a different photodissociation energy partitioning mechanism is involved. It is also possible that since $CH_2(^1A_1)$ is produced with higher energy at 229 nm, it loses a larger fraction of its energy to unreactive collisions. In fact, it is possible that the statistical model gives much narrower and lower average energy $CH_2(^1A_1)$ distributions than does CH_2N_2 photodissociation at any wavelength and that unreactive collisional energy loss, which may increase with increasing energy, gives reacting $CH_2(^1A_1)$ distributions similar to the statistical model at 436, 366, and 337 nm and much narrower than the statistical model distribution at 229 nm.

Statistical model calculations for the deuterated systems are presented as k_4 vs. S/D curves in Figure 6 for CD_2CO 214-nm photolyses and in Figure 7 for CD_2N_2 366-nm photolyses. In both cases the statistical model gives slightly narrower and lower average energy $CD_2(^1A_1)$ distributions than the data. The statistical model does qualitatively predict the broader and higher average energy distributions for $CD_2(^1A_1)$ relative to $CH_2(^1A_1)$; however, the magnitude is somewhat less than experimentally found. This is especially true for 214-nm ketene photolyses. A possible explanation is that $CH_2(^1A_1)$ may undergo more V–V transfer type collisional relaxation prior to reaction than does $CD_2(^1A_1)$ since the bath gases are rich in C–H bonds.[18] Other explanations such as possible uncertainties in the data and possible inadequacies of the statistical model cannot be ruled out.

If the frequencies of the remainder of the dissociating molecules were lowered, as expected for an activated complex, the statistically calculated distributions would be even narrower than those found here. The formation of $CH_2(^1B_1)$, which is energetically possible for ketene photolyses at 214 nm and diazomethane photolyses at 229 nm, can neither be ruled out nor confirmed by the present results since plausible explanations of the data are possible for either case.

Acknowledgment. We acknowledge the support of the National Science Foundation in the earlier phase of this work as well as the Southwest Resource Center in the later phase.

Registry No. MCB, 598-61-8; CB, 287-23-0; CH_2CO, 463-51-4; CD_2CO, 4789-21-3; CH_2N_2, 334-88-3; CD_2N_2, 14621-84-2; CH_2, 2465-56-7; CD_2, 14863-68-4.

(16) S. Yamabe and K. Morokuma, *J. Am. Chem. Soc.*, **100**, 7551 (1978).
(17) S. Yamabe, T. Minato, and Y. Osamura, *Int. J. Quantum Chem.*, **16**, 243 (1980).
(18) J. D. Lambert, "Vibrational and Rotational Relaxation in Gases", Oxford University Press, Oxford, England, 1977.

Oscillations and Oligo-Oscillations in Hydrogen Ion Concentration

Mihály T. Beck* and Gyula Rábai

Department of Physical Chemistry, Kossuth Lajos University, Debrecen, 10, Hungary 4010
(Received: January 31, 1985)

In different three oligoscillatory systems, the concentration of the hydrogen ion as a function of time shows a number of extrema: in the iodate–sulfite–malonic acid system, three, in the iodate oxidation of hydroxylamine, two, and in the iodate oxidation of thiourea as many as four extrema have been found in unbuffered solutions. Temporal oscillation of both the hydrogen ion concentration and the redox potential have been measured in the unbuffered chlorite–thiosulfate reaction in CSTR.

In the past two decades a great number of oscillatory[1] and recently a few oligo-oscillatory reactions[2-5] were discovered. In all published cases the reactions take place in either very acidic or buffered solutions, therefore the pH is practically constant while the concentrations of certain species exhibit in case of oligo-os-

(1) R. J. Field and M. Burger, Eds. "Oscillations and Traveling Waves in Chemical Systems", Wiley-Interscience, New York, 1984.
(2) Gy. Rábai, Gy. Bazsa, and M. T. Beck, *J. Am. Chem. Soc.*, **101**, 6746 (1979).
(3) Gy. Rábai, Gy. Bazsa, and M. T. Beck, *Int. J. Chem. Kinet.*, **13**, 1277 (1981).
(4) M. T. Beck and Gy. Rábai, *J. Chem. Soc., Dalton Trans.*, 1687 (1982).
(5) Gy. Rábai and M. T. Beck, *J. Chem. Soc., Dalton Trans.*, in press.

0022-3654/85/2089-3907$01.50/0